Dalton Transactions

An international journal of inorganic chemistry

rsc.li/dalton
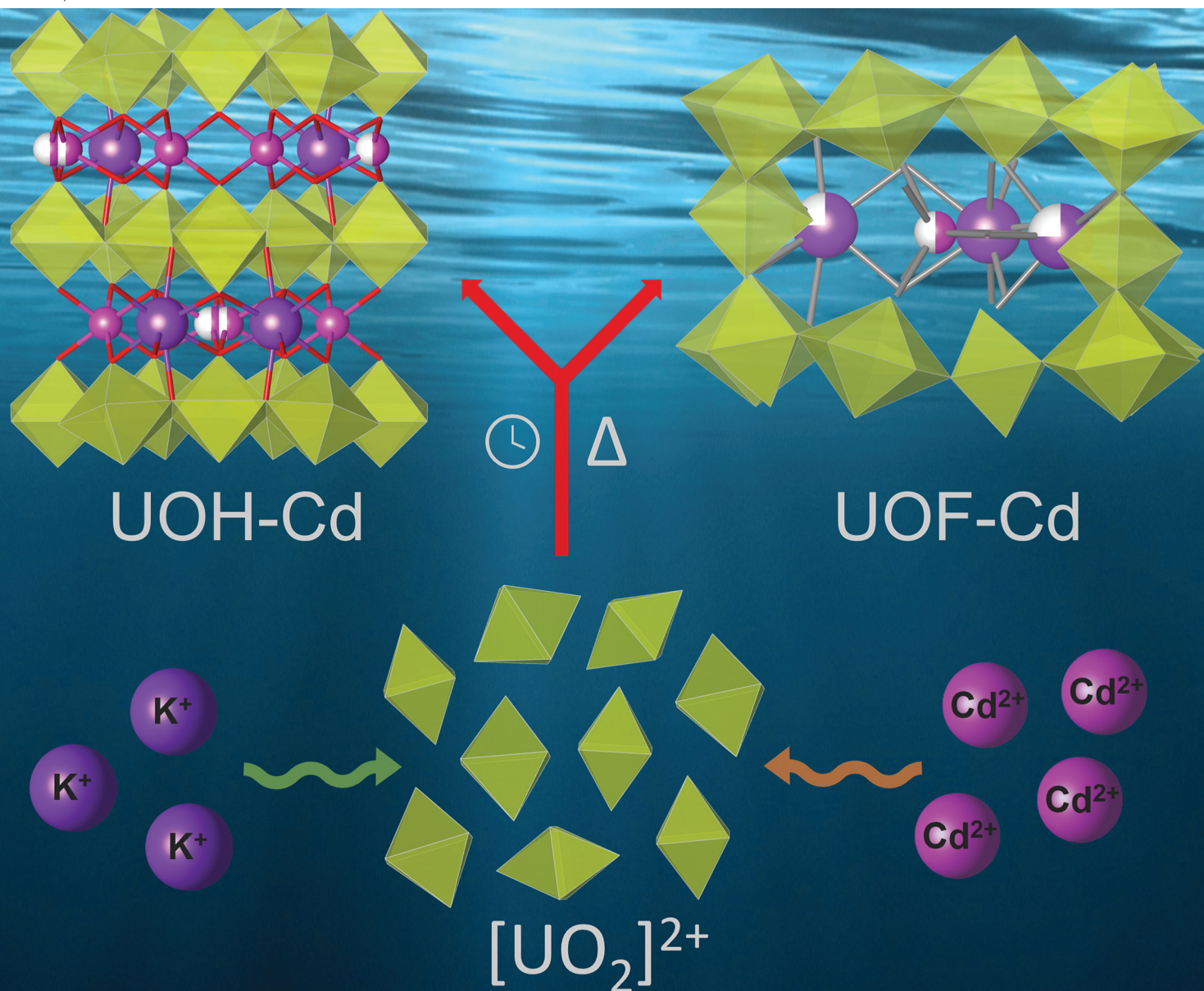
UOH-Cd

UOF-Cd

$[UO_2]^{2+}$

K⁺

K⁺

K⁺

Cd²⁺

Cd²⁺

Cd²⁺

Cd²⁺

Cd²⁺

ROYAL SOCIETY OF CHEMISTRY

PAPER
Yingjie Zhang *et al.*
Exploring the influence of pH on the structural intricacies of
uranium oxide hydrates containing both Cd(ii) and K(i) ions

PAPER

Check for updates

Exploring the influence of pH on the structural intricacies of uranium oxide hydrates containing both Cd(ii) and K(i) ions †

Timothy A. Ablott, Kimbal T. Lu, Tao Wei and Yingjie Zhang ID *

We report the synthesis of two new dual-cation uranium oxide hydrate (UOH) materials, containing both Cd^{2+} and K^+ ions, along with their characterisation by means of single-crystal X-ray diffraction and a range of other structural and spectroscopic techniques. The materials were found to differ in structures, topology and uranium to cation ratios, with the layered **UOH-Cd** crystallising in a plate morphology and containing a U : Cd : K ratio of 3 : 1.5 : 1. Conversely, the framework-type **UOF-Cd** incorporates much less Cd, with a U : Cd : K ratio of 4.4 : 0.2 : 1 and is found as needle-like crystals. A common feature in both structures is the presence of β-U_3O_8 type layers with a distinct uranium centre which lacks the expected uranyl bonds, highlighting the importance of the β-U_3O_8 layer in the subsequent self-assembly and preferential formation of a variety of structural types. Most importantly, by exploiting the additional flexibility provided by monovalent cation species (*i.e.*, K^+) as secondary metal cations to synthesise these novel dual-cation materials, this work highlights the potential for broadening the scope of viable synthetic UOH phases towards furthering the understanding of these systems in their roles as alteration products in the surrounds of spent nuclear fuel in deep geological repositories.

1. Introduction

The need to understand uranium oxide-based chemistry is ever present, principally due to its use as a nuclear fuel around the world.[1,2] With an ever-increasing need for cleaner energy sources, many countries have turned to nuclear energy to achieve the goal of reducing carbon emissions.[1,2] As a result, the study of uranium oxide compounds, both naturally occurring and synthetically derived, is of particular interest. With a drive to increased nuclear energy production comes an increase in the amount of spent nuclear fuel (SNF) being produced.[3] The current methods of safe SNF disposal are varied, however the most straightforward and thus often the most widely utilised is the storage of the SNF in stable geological repositories.[2] In these repositories, SNF is most commonly found in the form of UO_2, which when stored under reducing environments are insoluble and thus should remain confined within the repository. However, if exposed to oxygen and air, there exists the possibility of alteration by oxidation and/or

hydration, giving rise to the need to study these processes further.[4,5]

When exposed to these oxidative conditions, UO_2 species are known to oxidise from U^{4+} to U^{6+}. In their 6+ state uranium species, existing as uranyl $[(UO_2)^{2+}]$ cations, readily react with their environment to form uranyl oxide-containing compounds.[6,7] Given the strongly bonded axial oxygen atoms, these compounds typically form layers extending along their equatorial positions in tetragonal, pentagonal and hexagonal bipyramidal geometries. This results in the formation of materials containing uranyl polyhedra layers (sheets), between which lie interlayer cation species which are present in the environment of the repository.[8,9] Given their compositions, these compounds are given the name uranium oxide hydrates (UOH).[10]

The importance of understanding these materials has given rise to dozens of UOH-based minerals,[1,10,11] with more than a dozen synthetic UOH compounds having also been identified.[12–14] One of the main factors differentiating these materials is the secondary metal ion which lies between the uranyl oxide hydroxide layers, with a diverse range including alkali,[15] alkaline earth,[16] heavy metals,[17] transition metals[18] and lanthanides[19] having been reported thus far.

Complicating matters further is the possible formation of a UOH sub-structure, wherein the UOH takes on a framework-like orientation with uranyl species acting as bridging ligands

Australian Nuclear Science and Technology Organisation, Locked Bag 2001, Kirrawee DC, NSW 2232, Australia. E-mail: yzx@ansto.gov.au

between the uranyl polyhedra layers to form uranium oxide frameworks (UOFs). This results in the creation of channels within which lie the secondary metal species, which have proven capable of incorporating a range of secondary cations including Cs^+, Pb^{2+}, Sr^{2+}, Y^{3+}, Er^{3+}, Sm^{3+}, Eu^{3+}, Gd^{3+} and U^{4+}.[20–26] The additional complexity which UOFs introduce into understanding the chemistry of UO_2 in the environs of these geological repositories exemplifies the need to study these materials further.

The driving force in this field is the possible cations which may be present in the surrounds of these geological repositories. Cadmium, being relatively rare in the environment, has accordingly been unexplored for these UOH materials. However, given cadmium is the most soluble of the heavy metals in water,[27] there is a distinct possibility that the amount of cadmium in groundwater will increase due to ongoing anthropogenic activities.[27,28] Whilst anthropogenic activities are likely to vary over the expected timeframe of SNF exposure to groundwater, in a worst case scenario where the contaminated groundwater is introduced into the surrounding environment of a geological repository earlier than expected, there is the possibility that Cd^{2+} ions may play a role in the phase formations or alterations of UO_2 systems in these repositories.[29]

As of yet no Cd-based UOH systems, either synthetic or naturally occurring, have been reported in the literature, however the synthesis of UOH compounds containing 2+ transition metal species have proven successful (Table 1). Understanding whether Cd-based systems, given cadmium has a larger ionic radius compared to these 2+ transition metals, will also form under these synthetic conditions is therefore crucial to better understand its chemistry if introduced to the SNF environment.

An additional consideration is the abundance of potassium in the earth's crust, which ensures that K^+ ions will be present during any alteration or phase formation processes. Dual K^+-metal systems have been reported in a small number of UOH minerals[31,32] and synthetic phases.[18] However the role that potassium plays in possibly stabilising these UOH/F structures needs to be better understood. The larger charge density of many of the previously identified secondary ions, such as lanthanides, excludes the possible inclusion of K^+ into UOF structures. However, Cd^{2+} ion, having a smaller charge density, should also allow for potassium to be incorporated into the

structure, which may aid in understanding its role in the possible alteration chemistry of SNF.

Herein we report the syntheses of two novel synthetic UOH/F compounds and explore the effect of synthetic conditions on their structure evolutions. The crystals isolated from the hydrothermal reaction of uranyl nitrate with Cd^{2+} and K^+ ions were found to exist as either a layered UOH material or a framework-type structure. The U : Cd : K ratios, as determined through synchrotron single crystal X-ray diffraction analysis, was found to differ significantly between the two compounds. Their physical and spectroscopic properties were subsequently explored using scanning and transmission electron microscopy along with Raman and diffuse reflectance spectroscopy.

2. Experimental

2.1. Syntheses of materials

Uranyl nitrate hexahydrate with natural uranium was used in the synthesis of the materials. Compounds with uranium are radioactive and should be handled in the regulated laboratory. All other chemicals in A.R. grade were from Sigma-Aldrich (Merck).

2.1.1 $Cd_3K_2[(UO_2)_6O_9(OH)_2]$ (UOH-Cd). Cadmium nitrate tetrahydrate, $Cd(NO_3)_2·4H_2O$ (0.0308 g, 0.1 mmol) and uranyl nitrate hexahydrate (0.049 g, 0.1 mmol) were dissolved in 5 mL deionized (DI) water, followed by adjustment of the solution pH with KOH until the solution pH was 6.13. The solution was then transferred into a 30 mL Teflon vessel, sealed in a steel autoclave and heated in an oven at 240 °C for 24 h. Large orange plate crystals of compound **UOH-Cd** were obtained after cooling to room temperature at 5 °C h^{-1} with the final solution pH 5.40. The crystals of compound **UOH-Cd** were separated manually from a powdered material with ~30 wt% yield.

2.1.2 $Cd_1K_5(H_2O)_6[(UO_2)_{22}O_{23}(OH)_5]$ (UOF-Cd). Cadmium nitrate tetrahydrate, $Cd(NO_3)_2·4H_2O$ (0.0308 g, 0.1 mmol) and uranyl nitrate hexahydrate (0.049 g, 0.1 mmol) were dissolved in 5 mL DI water, followed by adjustment of the solution pH with KOH until the solution pH was 7.15. The solution was then transferred into a 30 mL Teflon vessel, sealed in a steel autoclave and heated in an oven at 240 °C for 24 h. Small orange needle crystals of compound **UOF-Cd** were obtained after cooling to room temperature at 5 °C h^{-1} with the final solution pH 5.95. The crystals of compound **UOF-Cd** were manually separated from a powdered material with ~20 wt% yield.

2.2. Characterisations

2.2.1. Synchrotron single crystal X-ray diffraction. The single crystal data for compounds **UOH-Cd** (CCDC 2244533†) and **UOF-Cd** (CCDC 2244534†) were collected at 100(2) K on the MX2 beamline[33] at the Australian Synchrotron employing silicon double crystal monochromated synchrotron radiation (λ = 0.71089–0.71093 Å). Data integration and reduction were

Table 1 Selected synthetic uranium oxide hydrate materials containing 2+ transition metals

UOH-TM^{2+}	Chemical formula	Space group
UOH-Mn[14]	$[Mn(H_2O)_4][(UO_2)_3O_3(OH)_2]·H_2O$	$P\bar{1}$
UOH-Zn[14]	$[Zn(H_2O)_4][(UO_2)_3O_3(OH)_2]·H_2O$	$P\bar{1}$
UOH-Ni[14]	$[Ni(H_2O)_4][(UO_2)_3O_3(OH)_2]·H_2O$	$P\bar{1}$
UOH-Co[14]	$[Co(H_2O)_4][(UO_2)_3O_3(OH)_2]·H_2O$	$P\bar{1}$
UOH-Ni[30]	$[Ni(H_2O)_4]_3[U(OH,H_2O)(UO_2)_8O_{12}(OH)_3]$	$P\bar{1}$
UOH-KNi[18]	$K_4Ni(OH)_3(H_2O)_9[(UO_2)_{12}O_7(OH)_{13}]$	$P3_1c$
UOH-KCo[18]	$K_4Co(OH)_3(H_2O)_9[(UO_2)_{12}O_7(OH)_{13}]$	$P3_1c$

undertaken with XDS.[34] Absorption corrections were applied to the data using SADABS.[35] The structures were solved by direct methods[36] and refined with SHELXL-2014[37] using the Olex[2] graphical user interface.[38] All atoms with ≥0.5 occupancies were located on the electron density maps and refined anisotropically. Hydrogen atoms on hydroxyl groups and water molecules were unable to be located and they were omitted in the structure refinements. Both compounds contain U as a strong X-ray absorber. In addition, the one-circle goniometer setup on the MX2 beamline provided less redundant data for absorption corrections. As such there were some Q-peaks around U atoms due to the ineffective absorption corrections.

2.2.2. Scanning electron microscopy (SEM) and transmission electron microscopy (TEM). The crystal morphologies and elemental compositions were analysed using SEM coupled with energy dispersive spectrometry (EDS). Samples were carbon coated and examined in a Zeiss Ultra Plus scanning electron microscope (Carl Zeiss NTS GmbH, Oberkochen, Germany) operating at 15 kV equipped with an Oxford Instruments X-Max 80 mm^2 SDD X-ray microanalysis system. EDS multipoint analyses were carried out on relatively flat crystal surfaces with Cu standard for calibration. Small amounts of finely ground, via mortar and pestle, crystal fragments were suspended in ethanol and then dispersed on a TEM holey-carbon film with copper support. The specimen was then characterized using a JEOL 2200FS (JEOL Ltd, Japan) TEM operated at 200 kV, fitted with an Oxford X-Max silicon drift detector for energy dispersive X-ray analysis (EDS). EDS data were analysed using the Oxford INCA v.4.15 microanalysis software.

2.2.3. Raman spectroscopy. Raman spectra were collected on a Renishaw inVia spectrometer equipped with a 785 nm excitation Ar laser in the range of 2000–100 cm^{-1} with a spectral resolution of ~1.7 cm^{-1}.

2.2.4. Diffuse reflectance spectroscopy (DRS). Absorption spectra in both the UV-visible and near-infrared (NIR) regions were recorded on an Agilent Cary 5000 spectrophotometer equipped with a Labsphere Biconical Accessory and referenced to a Labsphere certified standard.

3. Results and discussion

3.1. Material syntheses and microstructures

UOH-Cd and **UOF-Cd** were successfully synthesized under hydrothermal conditions, with uranyl nitrate as the uranium precursor and the pH adjustments achieved using a diluted KOH solution. **UOH-Cd**, isolated as yellow-orange crystals (Fig. S1, ESI†), formed after dissolving equimolar amounts of $Cd(NO_3)_2 \cdot 4H_2O$ and $UO_2(NO_3)_2 \cdot 6H_2O$ in H_2O, adjusting the solution pH to 6.13 and heating the solution to 240 °C for 24 h. The formation of **UOF-Cd**, also existing as yellow-orange crystals (Fig. S1, ESI†), was accomplished in a similar manner, with an aqueous solution containing equimolar amounts of $Cd(NO_3)_2 \cdot 4H_2O$ and $UO_2(NO_3)_2 \cdot 6H_2O$ in H_2O instead adjusted to a solution pH of 7.15 prior to heating to 240 °C for 24 h.

SEM-EDS analysis of **UOH-Cd** confirmed the presence of a single crystal morphology present as large plates (Fig. 1(a), left). EDS analysis confirmed the presence of U, Cd, K and O, with the U : Cd : K atomic ratios of 3 : 1.5 : 1 (Fig. 1(a), right; Fig. S2, ESI†). These ratios match those expected for layered UOH materials, with uranium to metal ratios of 2 : 1–4 : 1 most typically observed.[19,39,40] The PXRD pattern matches the calculated pattern from the single crystal data (Fig. S3, ESI†) suggesting a pure phase compound was obtained.

Immediately apparent in the SEM-EDS analysis of **UOF-Cd** (Fig. 1b) is the presence of two crystal morphologies, with the major phase existing as needle-like crystals (Fig. 1(b), left) and the minor phase as smaller plates (Fig. S4, ESI†). The presence of U, Cd and K was confirmed with EDS (Fig. 1(b), right; Fig. S4, ESI†), however the exact ratios could not be determined in this material due to the overlapping of major energies for U, Cd and K. In being unable to differentiate the energies of Cd and K from the U, which is suspected to exist as the major element in the material, this strongly suggests that the U : M (Cd/K) ratio is much higher than that observed in **UOH-Cd** and thus U dominates the EDS spectrum (Fig. S4, ESI†). With the needle-like morphology of the major phase matches those observed for previously reported UOF phases,[24–26] the expected U:M ratio would be ~5.5 : 1, which would explain the inability to obtain a definitive EDS spectrum for the trace amounts of Cd. The PXRD pattern of manually separated **UOF-Cd** matches the pattern calculated from its single crystal data (Fig. S5, ESI†), confirming its presence as the major phase. EDS analysis of the minor phase revealed U : Cd : K ratios akin to those observed in **UOH-Cd** ((Fig. S4(b), ESI†), confirming that the minor phase is that of a layered UOH material comparable to **UOH-Cd**. Given the relatively close solution pH between the two syntheses, **UOF-Cd** existing as a mixed phase is not unexpected. Some of the previously published UOFs have been reported as existing in a mixed phase system, with the UOF present as the major phase.[23]

In exploring the possible reason as to why the framework-type structure was favoured during the **UOF-Cd** synthesis, the most apparent conclusion is the solution pH. Past research has shown the influence the solution pH has on the formation of UOH compounds.[12,24] Interestingly, in those examples the lower solution pH drove the formation of a UOF material with higher solution pH giving rise to a layered structure instead. For these Cd-based systems, the trend appears reversed, with the higher pH driving the framework assembly. One possible alternative explanation is the increased K$^+$ concentration in solution during **UOF-Cd** formation, resulting from an increased amount of KOH required to increase the starting pH.

Given the EDS spectra shows that **UOF-Cd** contains a higher proportion of K$^+$ compared to that of **UOH-Cd**, it is possible that this influenced the final structure by providing a means of charge balance without the need to incorporate further Cd^{2+} ions. Thus K$^+$ ions appear to play a key role in the formation of UOF phase incorporating Cd^{2+} ions. Clearly illustrated is the elaborate chemistry for the formation of these UOH/F materials, hence the need to further the studies in this area.
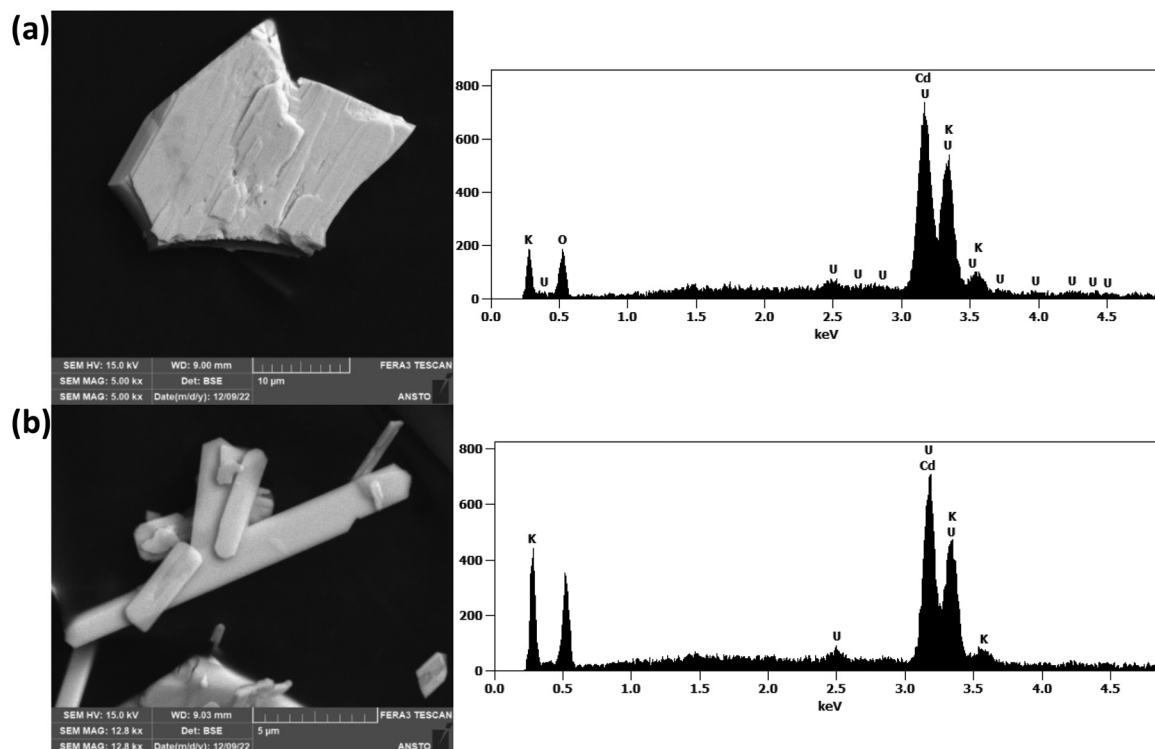
Fig. 1 SEM analysis of **UOH-Cd** (a) and **UOF-Cd** (b): backscattered SEM images of the crystals on the left and their corresponding EDS spectra on the right, confirming the presence of U, Cd and K in the crystals.

3.2. Crystal structures and discussion

The crystal data and refinement details for **UOH-Cd** and **UOF-Cd** are summarised in Table 2. Selected bond lengths (Å) and angles (°) are provided in Tables 3 and 5, with calculated bond valence sums (BVSs)[9] presented in Tables 4 and 6 with parameters for U^{6+}, Cd^{2+} and K^+ taken from the literature.[9,41,42]

Table 2 Crystal data and structure refinement details for compounds **UOH-Cd** and **UOF-Cd**

Compound	**UOH-Cd**	**UOF-Cd**
CCDC	2244533†	2244534†
Empirical formula	$Cd_3K_2O_{23}U_6$	$Cd_{0.5}K_{2.5}O_{39}U_{11}$
Formula weight	2211.58	3396.28
Crystal system	Orthorhombic	Monoclinic
Space group	$Pnnm$	$C2/c$
a (Å)	12.398(3)	11.589(2)
b (Å)	7.0070(14)	21.125(4)
c (Å)	11.482(2)	14.596(3)
$\alpha/(°)$	90	90
$\beta/(°)$	90	104.23(3)
$\gamma/(°)$	90	90
Volume (Å^3)	997.5(3)	3463.8(13)
Z/μ (mm^{-1})	2/52.169	4/6.513
Min./Max. θ [°]	4.836/51.998	3.856/49.992
d_{calcd} (g cm^{-3})	7.363	6.513
GOF	1.081	1.114
Final R_1 ^{a} [$I > 2\sigma(I)$]	0.0294	0.0538
Final wR_2 ^{b} [$I > 2\sigma(I)$]	0.0814	0.1327

^{a} $R_1 = \Sigma||F_o| - |F_c||/|F_o|$; ^{b} w$R_2 = \Sigma[w(F_o{}^2 - F_c{}^2)^2]/\Sigma[w(F_o{}^2)^2]^{1/2}$.

UOH-Cd crystallises in the orthorhombic $Pnnm$ space group, with the asymmetric unit containing two distinct U centres, two Cd centres (Cd1 in full and Cd2 in half occupancies) and a full occupancy K site. The U1, Cd2 and K1 sites are modelled with partial occupancies due to lying on Wyckoff positions. U1 exists in a distorted octahedral geometry and U2 in a pentagonal bipyramidal geometry. Both Cd1 and Cd2 exist in a 6-coordinate distorted octahedral geometry, with the K species present as an 8-coordinate square antiprism.

Exploring the full structure reveals that the material exists as a layered structure made up of 2D sheets constructed from the U polyhedra, with the secondary Cd^{2+} and K^+ ions lying between these layers (Fig. 2(a)). The uranyl polyhedra layer exists as a β-U_3O_8-type structure, with the pentagonal bipyramidal U2 centres forming continual chains via O–O edge-sharing which are bridged by the U1 octahedra (Fig. 2(b)). The coordination sphere about U2 shows the expected U=O bond lengths of 1.858(7) Å (O6) and 1.885(6) Å (O5) at the axial positions, with a nearly linear O=U2=O bond of 178.5(3)°. The equatorial U–O bonds (O3, O4 and O7), which participate in the O–O edge-sharing, fall in the range of 2.289(8) Å–2.397(7) Å, consistent with the observed values for uranyl polyhedra in these systems.[8,30,43] The coordination environment about U1 is unusual in that it does not involve a uranyl species, with U–O bond lengths of 1.974(9) Å to 2.127(6) Å observed in the axial positions. Whilst uncommon, similar results have been found in other synthetic UOH systems.[9,21,30,44]

Table 3 Selected bond lengths (Å) and angles (°) for **UOH-Cd**

UOH-Cd							
U1–O1	1.974(11)	U2–O4[6]	2.350(7)	Cd1–O5[10]	2.284(6)	K1–O1[3]	2.864(8)
U1–O2	1.996(9)	U2–O4	2.289(8)	Cd1–O5[6]	2.284(6)	K1–O1[7]	2.864(8)
U1–O3[5]	2.127(6)	U2–O5	1.885(6)	Cd1–O6[11]	2.344(7)	K1–O3[7]	2.743(7)
U1–O3	2.127(6)	U2–O6	1.858(7)	Cd1–O6	2.344(7)	K1–O3[13]	2.743(7)
U1–O4[5]	2.116(7)	U2–O7	2.132(2)	Cd2–O1[3]	2.113(11)	K1–O5	2.830(7)
U1–O4	2.116(7)	O6=U2=O5	178.5(3)	Cd2–O1	2.113(11)	K1–O5[14]	2.830(7)
U2–O3[7]	2.301(7)	Cd1–O2[9]	2.257(6)	Cd2–O5	2.544(7)	K1–O6[15]	2.775(8)
U2–O3[6]	2.397(7)	Cd1–O2[7]	2.257(6)	Cd2–O5[13]	2.544(7)	K1–O6[6]	2.775(8)

[1]$1/2 − X, −1/2 + Y, 1/2 + Z$; [2]$1/2 − X, −1/2 + Y, 1/2 − Z$; [3]$−X, 1 − Y, 1 − Z$; [4]$+X, −1 + Y, +Z$; [5]$+X, +Y, 1 − Z$; [6]$1/2 − X, 1/2 + Y, 1/2 − Z$; [7]$+X, 1 + Y, +Z$; [8]$1 − X, 2 − Y, 1 − Z$; [9]$1 − X, 1 − Y, 1 − Z$; [10]$1/2 + X, 3/2 − Y, 1/2 − Z$; [11]$1 − X, 2 − Y, +Z$; [12]$−X, 2 − Y, 1 − Z$; [13]$−X, 1 − Y, +Z$; [14]$−X, 2 − Y, +Z$; [15]$−1/2 + X, 3/2 − Y, 1/2 − Z$.

Table 4 BVS calculations for **UOH-Cd**

	U1		U2		Cd1		Cd2		K1			
Occ.	**1**		**1**		**1**		**0.5**		**1**			
Sym.	**2**		**1**		**1**		**2**		**2**			
CN	**6**		**7**		**6**		**6**		**8**		**Σ**	
O1	1.16						0.56	0.56	0.13	0.13	**1.86**	
O2	1.11				0.38	0.38					**1.50**	
O3	0.86	0.86			0.62	0.51			0.18	0.18	**2.18**	
O4	0.88	0.88			0.56	0.63					**1.45**	
O5			1.38		0.36	0.36	0.35	0.35	0.14	0.14	**2.24**	
O6			1.45		0.30	0.30			0.17	0.17	**1.92**	
O7			0.85								**0.86**	(OH)
O8											**0.00**	(H$_2$O)
Σ	**5.77**		**6.01**		**2.09**		**1.84**		**1.25**			

Table 5 Selected bond lengths (Å) and angles (°) for **UOF-Cd**

UOF-Cd							
U1–O1[1]	2.271(19)	U2–O2	2.439(14)	U3–O7	2.208(14)	U4–O3[2]	2.389(13)
U1–O1	2.271(19)	U2–O3	2.439(15)	U3–O8	1.932(16)	U4–O10	2.301(14)
U1–O2	2.005(14)	U2–O4	1.773(15)	U3–O9	1.813(14)	U4–O10[5]	2.249(14)
U1–O2[1]	2.005(14)	U2–O5	1.805(16)	U3–O10	2.200(14)	U4–O11	2.284(14)
U1–O3	1.982(14)	U2–O6[2]	2.29(3)	U3–O11	2.186(14)	U4–O12	1.951(16)
U1–O3[1]	1.982(14)	U2–O7	2.326(14)	U3–O19[5]	2.200(13)	U4–O13	1.833(15)
		U2–O11[2]	2.296(14)	O9=U3=O8	176.2(7)	U4–O14	2.213(16)
		O4=U2=O5	177.9(7)			O13=U4=O12	176.3(7)
U5–O8[4]	2.379(16)	U6–O2[7]	2.438(14)	Cd1–O1	2.335(19)	K1–O4[11]	2.984(16)
U5–O12[4]	2.404(16)	U6–O7[7]	2.359(14)	Cd1–O1[9]	2.335(19)	K1–O4[2]	2.984(16)
U5–O12	2.480(16)	U6–O14	2.236(16)	Cd1–O5[10]	2.581(17)	K1–O9	2.919(15)
U5–O14	2.319(16)	U6–O17	1.798(14)	Cd1–O5[1]	2.581(17)	K1–O9[12]	2.919(15)
U5–O15	1.781(14)	U6–O18	1.883(16)	Cd1–O20[9]	2.374(16)	K1–O13[12]	2.809(15)
U5–O16	1.777(14)	U6–O19[6]	2.309(13)	Cd1–O20	2.374(16)	K1–O13	2.809(15)
U5–O18	2.437(14)	U6–O19	2.270(13)			K1–O15[5]	2.947(15)
O16=U5=O15	177.4(7)	O17=U6=O18	176.0(6)			K1–O15[13]	2.947(15)
K2–O8[7]	3.102(15)	K3–O4[18]	2.852(17)				
K2–O8[4]	3.102(15)	K3–O4	2.852(17)				
K2–O17[14]	2.726(15)	K3–O7[18]	2.931(15)				
K2–O17[6]	2.726(15)	K3–O7	2.931(15)				
K2–O18	2.685(16)	K3–O8	3.238(16)				
K2–O18[15]	2.685(16)	K3–O8[18]	3.238(16)				
K2–O20[16]	2.714(16)	K3–O18[3]	2.888(16)				
K2–O20[17]	2.714(16)	K3–O18[4]	2.888(16)				

[1]$3/2 − X, 3/2 − Y, 1 − Z$; [2]$1/2 − X, 3/2 − Y, 1 − Z$; [3]$1 + X, +Y, +Z$; [4]$−X, +Y, 3/2 − Z$; [5]$−X, 1 − Y, 1 − Z$; [6]$−1 − X, 1 − Y, 1 − Z$; [7]$−1 + X, +Y, +Z$; [8]$3/2 + X, 1/2 + Y, +Z$; [9]$2 − X, +Y, 3/2 − Z$; [10]$1/2 + X, 3/2 − Y, 1/2 + Z$; [11]$−1/2 + X, 3/2 − Y, −1/2 + Z$; [12]$−X, +Y, 1/2 − Z$; [13]$+X, 1 − Y, −1/2 + Z$; [14]$+X, 1 − Y, 1/2 + Z$; [15]$−1 − X, +Y, 3/2 − Z$; [16]$1/2 − X, −1/2 + Y, 3/2 − Z$; [17]$−3/2 + X, −1/2 + Y, +Z$; [18]$1 − X, +Y, 3/2 − Z$.

Table 6 BVS calculations for **UOF-Cd**

	U1		U2	U3	U4	U5		U6	Cd1		K1	K2	K3	Σ	
Occ.	1		1	1	1	1		1	0.5		1	0.75	0.75		
Sym.	2		1	1	1	1		1	2		2	2	2		
CN	6		7	6	7	7		7	6		8	8	8	Σ	
O1	0.65	0.65							0.31	0.31				0.97	(OH)
O2	1.09	1.09	0.47					0.47						2.04	
O3	1.14	1.14	0.47		0.52									2.14	
O4			1.71								0.19		0.27	2.17	
O5			1.61						0.16	0.16				1.77	
O6			0.63 x2											1.26	(OH)
O7			0.59	0.74				0.55					0.22	2.10	
O8				1.26		0.53						0.14	0.10	2.02	
O9				1.58							0.23			1.81	
O10				0.75	0.62	0.68								2.05	
O11			0.62	0.77	0.64									2.03	
O12					1.21	0.51	0.44							2.16	
O13				1.52							0.30			1.83	
O14				0.73	0.60			0.70						2.03	
O15						1.68					0.21			1.89	
O16						1.70								1.70	
O17								1.63				0.38		2.01	
O18					0.48			1.38				0.43	0.25	2.53	
O19			0.75					0.61	0.66					2.01	
O20									0.28	0.28		0.39		0.67	(H$_2$O)
Σ	5.78		6.11	5.85	5.93	5.93		6.00	1.51		0.93	1.34	0.83		

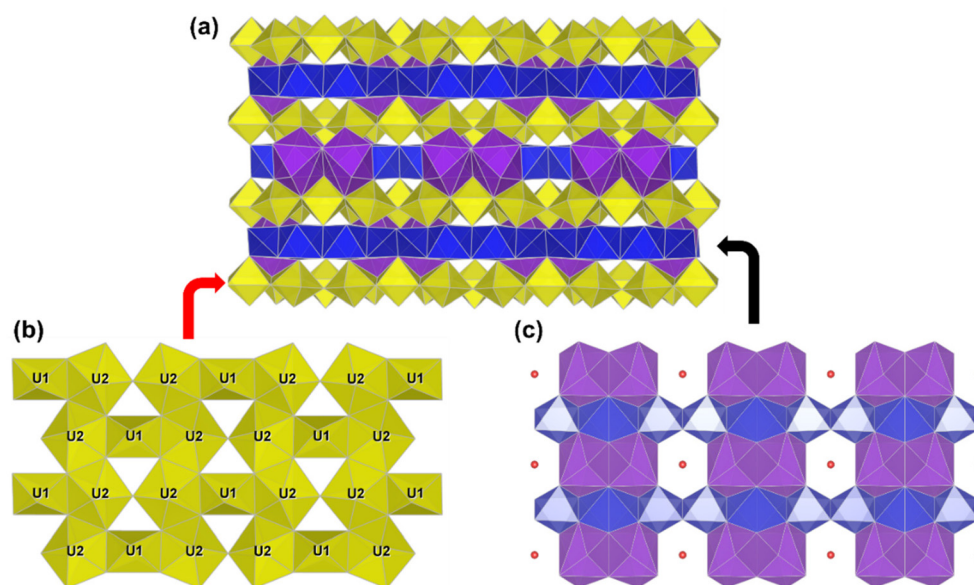**Fig. 2** Crystal structure of **UOH-Cd**: a polyhedral crystal structure along the *b*-axis (a), a polyhedral view of the uranyl oxide hydroxide layer with a β-U_3O_8 topology (b), and a polyhedral view of the Cd^{2+}/K^+ interlayer cations (c); U in yellow, Cd in blue and K in purple.

BVS calculations (Table 4) using the parameters reported by Burns *et al.* (R_{U-O} = 2.051; B = 0.519),[9] confirm that both U centres are present as U^{6+}, with the oxygen species existing majorly as O, with only O7 existing as OH which connects the adjacent U2-U2 chains. From this, the general formula for **UOH-Cd** was determined to be $Cd_3K_2[(UO_2)_6O_9(OH)_2]$.

The formation of a β-U_3O_8 sheet topology is intriguing as it is rarer in synthetic UOH materials, with an α-U_3O_8 layer more commonplace.[18,19,39,43,45] The β-U_3O_8 topology has been observed in a number of UOH minerals,[46–50] but much less in layered synthetic structures.[30,43] Interestingly, the β-U_3O_8 topology is overwhelming favoured in UOF materials,[20,23–26,44] likely due to the fact that the β-U_3O_8 anion topology can accommodate multiple valence states of uranium, a necessity in UOFs which contain mixed U^{5+}/U^{6+} sites within their structure.[23–25] Moreover, in the studies by Zhang *et al.*,[43] and Rivenet *et al.*,[30] wherein the uranyl polyhedra layers take on the β-U_3O_8 layout, the interlayer cations (Tb^{3+}/Ni^{2+}) act as

pillars which separate the uranyl polyhedra sheets. Each cation 'pillar' exists as an isolated species with channels in between, creating a pseudo-UOF material. The same trend is not immediately apparent in **UOH-Cd**, wherein the Cd^{2+} ions form chains, linking the layers *via* the axial O2 and O5 oxygens, and which lie perpendicular to U2–U2 chains in the uranyl polyhedra sheets (Fig. 2(c)). However, this Cd–Cd coordination is vastly different from that seen for other interlayer cation species in the literature in that it exists as 1D chains (Fig. 3(a)) as opposed to the 2D topologies seen for many UOH materials (Fig. 3(b)).[39,43] As a result, these Cd chains pillar the uranyl polyhedra sheets, with the chains themselves each linked through $K^+–K^+$ dimeric units (Fig. 2(c)), between which lies an isolated, unbound water molecule.

Interestingly, these Cd^{2+} pillars may also account for the different abundance of Cd : K compared to the rations reported in previous dual-cation systems. A study by Zhang and co-workers reported two dual-cation UOH materials containing both K^+ and either Co^+ or Ni^+, however with reported K : Co/Ni ratios of 3.5 : 1. Also revealed was the Co^{2+} and Ni^{2+} ions lay close to one of the β-U_3O_8 layers and were only coordinated to one U centre, with the K^+ ions linking the β-U_3O_8 sheets, which accounted for the observed K : Co/Ni ratio. The lower abundance of K^+ in **UOH-Cd** can therefore be attributed to the capability of Cd^{2+}, which has a larger ionic radius compared to both Co^{2+} and Ni^{2+}, to coordinate adjacent β-U_3O_8 layers.

SC-XRD confirmed the structure of **UOF-Cd** existed as a framework (Fig. 4(a)), with the material crystallising in the

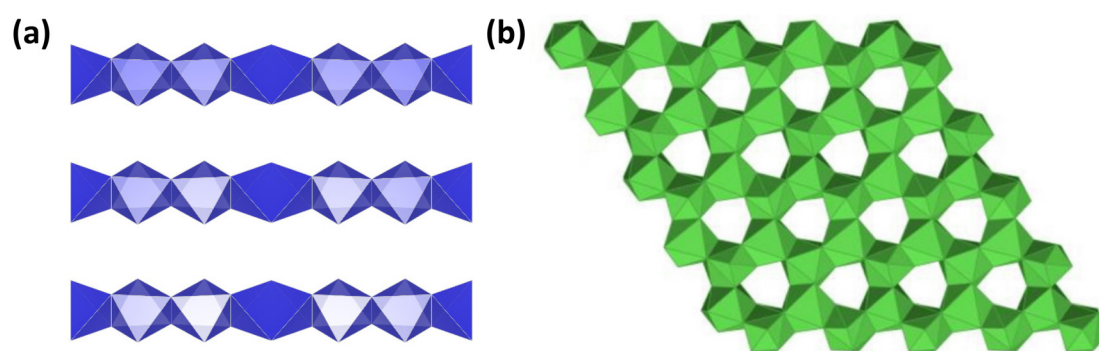**Fig. 3** A polyhedral view of the topology of the Cd–Cd chains in **UOH-Cd** (a) and the interlayer cation topology of U-La,[39] representative of the more commonly observed topology (b).
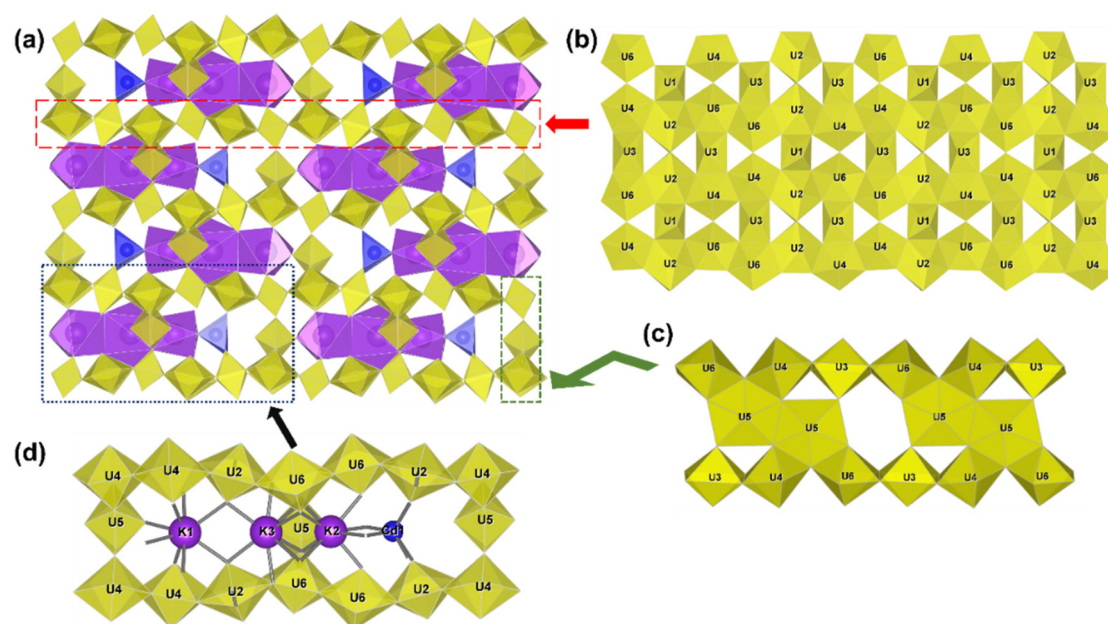

Fig. 4 Crystal structure of **UOF-Cd**: a polyhedral crystal structure along the *a*-axis (a), a polyhedral view of the uranyl oxide hydroxide layer with a β-U_3O_8 topology (b), the uranyl oxide hydroxide layers linked by double U5 pentagonal bipyramids (c), the 8-fold coordinated K^+ and 6-fold co-ordinated Cd^{2+} interlayer cations in the framework channels (d); U in yellow, Cd in blue and K in purple.

monoclinic $C2/c$ space group. The asymmetric unit was much larger, containing six unique U centres, one half occupancy Cd^{2+} site and three partial occupancy K^+ sites. The uranium centres each exist in full occupancies, with U1 modelled in half occupancies as it lies in a special position. The U sites take on two geometries, with U1 and U3 as 6-coordinate octahedra and U2, U4, U5 and U6 present as pentagonal bipyramids. The Cd ion lies in the channels of the framework in a trigonal prismatic geometry, with two of the K^+ centres taking on a bicapped trigonal prismatic geometry (K1 and K3), and one present as a square antiprism (K2).

The uranyl polyhedra sheets which make up the framework backbone is structurally similar to **UOH-Cd**, with the U centres taking on a β-U_3O_8-type layout. The U polyhedra are arranged to form chains of pentagonal bipyramids (U2, U4 and U6) through O–O edge sharing in a –(U2–U4–U4–U2–U6–U6–U2)– pattern (Fig. 4(b)). Each chain is antiparallel to the neighbouring sequence and are linked through U1 and U3 octahedra. Linking of the layers by discrete U5–U5 units through edge-sharing (U6/U4–U5) and corner-sharing (U2–U5) (Fig. 4(c)) completes the backbone of the framework-type structure.

Five of the six U centres (U2–U6) each have the expected pair of axial U=O bonds (1.773(15) Å–1.951(16) Å) with near linear bond angles (176.0°–177.9°). Of these, the pentagonal bipyramids each also coordinate five oxygens in their equatorial planes, with the octahedral U3 centre coordinating four O species. These equatorial bond lengths ranging from 2.186(14) Å to 2.480(16) Å are typical of previously reported UOF materials, falling within the same ranges.[23,24,26]

Curiously, as with **UOH-Cd**, the octahedral U1 does not contain any uranyl bonds, with all six bonds in the range of 1.982(14) Å to 2.271(19) Å. As discussed above, whilst this type of uranium centre has been observed in other materials, the same U species present in both materials strongly suggests that a correlation exists between **UOF-Cd** and the layered **UOH-Cd**. BVS values were calculated (Table 6) and confirmed that, as with **UOH-Cd**, all U centres existed as U^{6+}. Interestingly, this is divergent from many of the previously reported UOF structures which contain a mixed valence U^{5+}/U^{6+} at the same position as the U1/U3 octahedral sites observed in **UOF-Cd**. The previously reported presence of U^{5+} at this U1/U3 site within these framework-type structures, along with the fact that the same octahedral U species is near identical in both **UOH-Cd** and **UOF-Cd** strongly implies a link between the chemistry about this site and the preferred structure of the UOH/F material.

The oxygen species exist primarily as O, with one H_2O molecule (O20) shared between the Cd/K cations and two co-ordinated OH (O1 and O6), with the O6 site disordered in two positions. Based on the U and O types present, the material was formulated as $Cd_1K_5(H_2O)_6[(UO_2)_{22}O_{23}(OH)_5]$.

A unique feature of **UOF-Cd** is the coordination of the secondary cations within the channels of the framework. The K^+ and Cd^{2+} cations form a K1–K3–K2–Cd bonding motif, which lies across two channels of the framework, passing between the U5-U5 pillars (Fig. 4(d)). Each of the K centres is linked

through shared uranyl–cation interactions *via* the axial oxygen atoms of the U centres, with the Cd terminus coordinating K2 *via* both uranyl–cation interactions and a shared H_2O molecule (O20).

As a result of this secondary cation arrangement, **UOF-Cd** has a much higher abundance of K^+ compared to that of **UOH-Cd**, with a K : Cd ratio of 5 : 1 in the framework, compared to 3 : 2 in the layered structure. This secondary cation arrangement is particularly intriguing when compared to other framework-type structures in the literature. UOF materials containing Eu, Gd and Er, which have ionic radii comparable to those of Cd^{2+}, have all been reported as single-cation systems.[23,25] The obvious difference is therefore the oxidation state of the secondary cation species. With the presence of the secondary cations also driven by charge balance, the monovalent K^+ is therefore required to stabilise the framework structure. Whilst it has been hypothesised that the ionic radius of the secondary cations has an influence on the resultant structure, with the pore environment of UOF materials more readily impacted by the ionic radii of the secondary cations,[12] this result clearly demonstrates that for framework-type structures to be favoured, charge balance of the anion layer and the ionic radii of the secondary cations must both be accommodated.

Thus, it stands to reason that monovalent cations such as K^+, having comparable ionic radii to many of the cation species readily found in the environment (Ca^{2+}, Sr^{2+}, Zn^{2+}) as well as species found in the surrounds of SNF in an underground repository (Pb^{2+}, Ln^{3+}), could offer additional stability to UOH/F materials by providing an additional means of balancing the charge of their structures.

3.3. TEM characterization

Both compounds were further examined by TEM. For **UOH-Cd**, a TEM bright field image (Fig. 5a) showed a crushed grain. TEM-EDS analysis confirmed the presence of U, Cd and K. The SAED pattern (Fig. 5b) collected on the grain in zone axis of [1 1 0] was indexed to the orthorhombic *Pnnm* space group, consistent with the SC-XRD result. A HRTEM image in zone axis [6 3 1] from edge of the **UOH-Cd** grain showed lattice fringes with an inserted FFT image (Fig. 5c). The d (1 −2 0) spacing value of 0.337 nm measured from the image is consistent with the crystal data from SC-XRD. For **UOF-Cd**, a bright field TEM image (Fig. 6a) showed thin needle crystals. A SAED pattern in zone axis of [0 −1 3] is indexed to the monoclinic $C2/c$ space group (Fig. 6b). A HRTEM image in zone axis [0 −1 3] is showed in Fig. 6c with an inserted FFT image. The measured d (4 0 0) spacing value (0.281 nm) is consistent with the crystal data from SC-XRD.

3.4. Electronic structures and uranium valences

With UOH/F structures previously reported to contain U^{5+} centres within their structures,[22,23,26] DRS measurements were carried out to examine the uranium centres within both **UOH-Cd** and **UOF-Cd**. The presence of U^{5+} ($5f^1$) is typically confirmed by the appearance of peaks in the near infrared
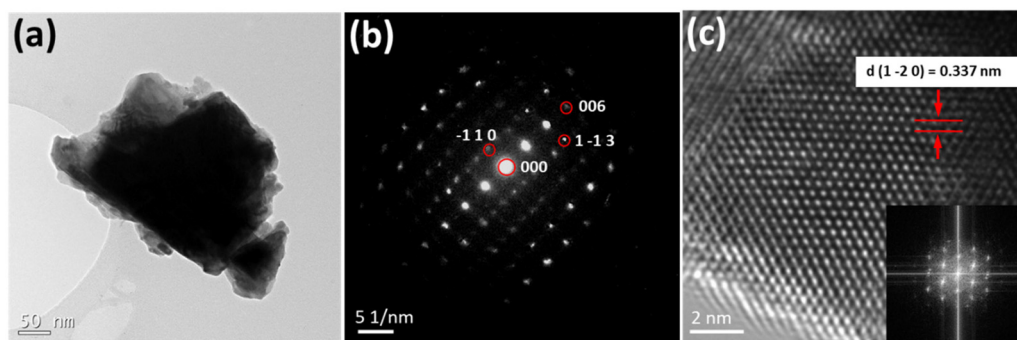
Fig. 5 TEM of **UOH-Cd**: (a) a TEM bright field image of a grain; (b) a SAED pattern of the grain in zone axis of [1 1 0] indexed to the orthorhombic *Pnnm* space group; and (c) a HRTEM image in zone axis [6 3 1] from edge of the grain with inserted FFT image.
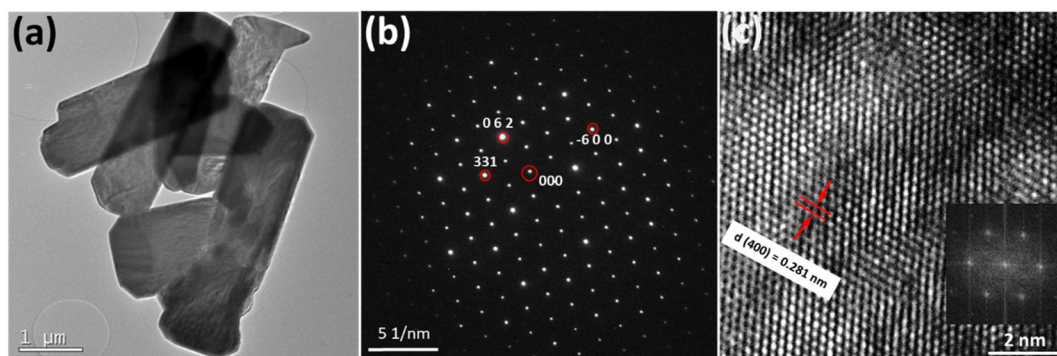

Fig. 6 TEM of **UOF-Cd**: (a) a bright field TEM image; (b) a SAED pattern of a grain in zone axis of [0 −1 3] indexed to the monoclinic *C*2/*c* space group; and (c) a HRTEM image with inserted FFT image in zone axis [0 −1 3].

region (1538–833 nm) resulting from crystal-field splitting of $^2F_{5/2}$–$^2F_{7/2}$.[26,51] Lacking any f electrons (5f^0), U^{6+} can only be distinguished by charge-transfer bands in the UV and far UV regions.

The most significant feature observed in both spectra (Fig. 7) is the broad, undefined absorption peaks in the UV region (220 nm–500 nm), correlating to the charge transfer bands of the U^{6+} centres in both materials. The only peaks of note in the NIR region are very weak and broad signals at ~1460 nm, most likely arising from trace amounts of water in the samples. Of significance is the lack of any sharp absorption peaks correlating to the presence of U^{5+} in either material, confirming the U centres exist in the 6+ state, as indicated by the BVS calculations (Tables 4 and 6).

3.5. Vibrational modes

Raman spectroscopy allows for the examination of the vibrational modes of **UOH-Cd** and **UOF-Cd**. As determined by past studies on UOH/F materials, peaks corresponding to the vibrational modes $\nu_1(UO_2)^{2+}$, $\nu(U_3O)/\gamma[U_3(OH)_3]$ and $\nu_2(UO_2)^{2+}$ should be visible in the region of 900–700 cm^{-1} as strong, sharp peaks, 300 to 600 cm^{-1} as medium intensity, broad peaks and 200–300 cm^{-1} as weak, broad peaks, respectively.[52–54]
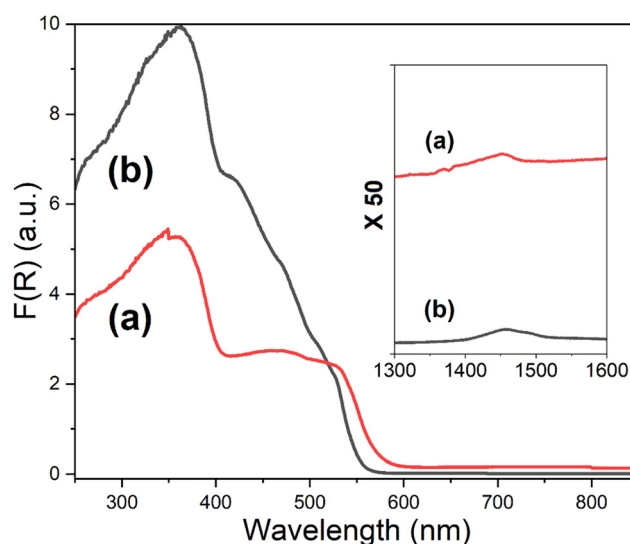

Fig. 7 The DRS spectra of **UOH-Cd** (a) and **UOF-Cd** (b) in the UV-vis region; inset is the same spectra in the near infrared region.

The spectrum for **UOH-Cd** (Fig. 8a) reveals two peaks at ~880 cm^{-1} and 860 cm^{-1}, corresponding to the U═O bonds of the bipyramidal U2. The bands at between 520–310 cm^{-1} are assigned to $\nu(U_3O)$ bridge elongations and $\gamma[U_3(OH)_3]$ bending
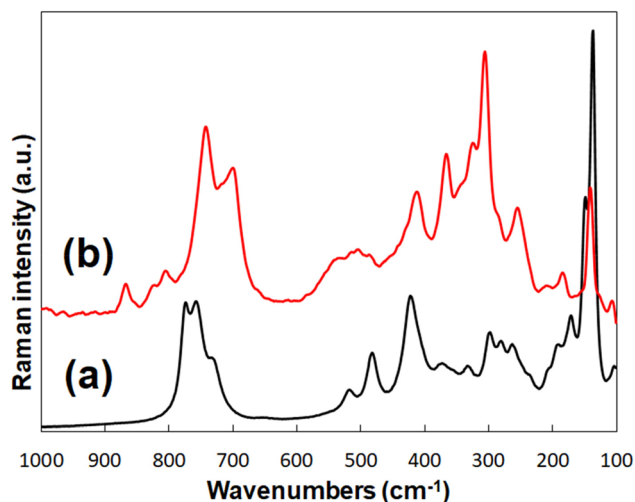
Dalton Transactions

View Article Online

Open Access Article. Published on 25 April 2023. Downloaded on 8/27/2025 10:16:11 PM. This article is licensed under a Creative Commons Attribution-NonCommercial 3.0 Unported Licence.

Fig. 8 The Raman spectra of **UOH-Cd** (a) and **UOF-Cd** (b).

vibrations, as well as possible $\nu(\text{U–O}_{\text{ligand}})$ vibrations. $\nu_2(\text{UO}_2)^{2+}$ bending vibrations account for the peaks between 295–200 cm^{-1}, with lattice vibrations giving rise to the intense, sharp peak at ~130 cm^{-1}.

Additional peaks are evident in the $\nu_1(\text{UO}_2)^{2+}$ region for **UOF-Cd** (Fig. 8b), due to the extra unique uranium centres present in the framework, with the peaks at 860, 810, 800, 750 and 705 cm^{-1} corresponding to the U=O bond lengths between 1.773 Å–1.951 Å. The additional peaks below this region are attributed to the same vibrational modes as assigned for **UOH-Cd**.

3.6. Implications and perspectives

The successful synthesis of both a layered UOH and a related UOF material, containing the same secondary cation species but varying greatly in their relative abundances, clearly highlights the need to explore more dual-metal UOH systems. Many UOH minerals containing dual-cations have been documented previously, however despite this only a few synthetic UOH materials have been reported. The formation conditions, seemingly driven by the solution pH during synthesis, have been clearly demonstrated to be more tolerant than previously reported, with the highest solution pH resulting in the formation of a framework-type structure reported thus far. Past studies have established that solution pH heavily influences the structure of the final products, as a result of the increasing proportion of hydrolysed uranyl species such as $[\text{UO}_2(\text{OH})]^+$, $[(\text{UO}_2)(\text{OH})_2]$, $[(\text{UO}_2)_2(\text{OH})_2]^{2+}$ and $[(\text{UO}_2)_3(\text{OH})_5]^+$ which form when solution pH is above 5. The apparent relationship between UOH and UOF structures, as evidenced by the near identical β-U$_3$O$_8$-type sheets present in both synthesised materials, highlights the seemingly delicate balance of reaction conditions which can lead to the preferred formation of one structure over the other. Future work towards exploring this balance, particularly targeting the entire pH range which gives rise to these hydrolysed species, is essential towards

intuiting the conditions that drive the preferential formation of these UOH/F phases.

The results of this work can be extended to encompass the alteration chemistry of UO$_2$ under the conditions which may be found for disposal of SNF in geological repositories. The significance of studying dual-cation systems has been demonstrated within this work, as shown by the varying ratios of Cd : K incorporated within the two structures. Given the formation conditions of UOF structures have been found to be more restrictive, the additional flexibility provided by a mixed-valence cation system could have a significant impact on the final products of the UO$_2$ alteration pathway under the repository conditions. Thus, these dual-metal systems warrant further study. In extending this work to other possible cations found within the surrounds of the SNF, a clear target is that of transition metals. Given their abundance in the environment, the understanding of the alteration chemistry of UO$_2$ systems in the presence of transition metals is essential. With only a handful of transition metal-containing UOH materials reported,[14,18,30] there exists a clear need for further study in this area.

Given the successful incorporation of K$^+$ alongside the Cd^{2+} species, work exploring other monovalent cations in dual-metal systems is also crucial. The most apparent choice to explore is that of Cs$^+$ ions, which will be present within the SNF and therefore a possible factor in the alteration of UO$_2$. A small number of UOH-Cs structures have been reported,[20,45] however exploring the Cs-system alongside other metals in a dual-cation system could prove insightful.

4. Conclusions

Two new UOH/F structures, each incorporating Cd^{2+} and K$^+$ in differing ratios, have been synthesised under hydrothermal conditions with uranyl nitrate as the U source. The layered UOH structure, which crystallised in the *Pnnm* space group, had a U : Cd : K ratio of 3 : 1.5 : 1. Comparatively, the framework-type structure, crystallising in the *C*2/*c* space group, had a much higher abundance of K$^+$, with a U : Cd : K ratio of 4.4 : 0.2 : 1. Both structures contained β-U$_3$O$_8$-type uranyl oxide hydroxide layers, consistent with previously reported framework-type structures but rare amongst layered structures. As both materials contained the near identical β-U$_3$O$_8$-type layers and a distinct octahedral U centre lacking the expected U=O bonds, this strongly suggested a close correlation between the two materials. Significantly, the increased abundance of K$^+$ in the UOF material suggests the inclusion of a second cation species with a different valence could be hugely impactful on the structure which eventuates from the synthesis.

These compounds further illustrate the sensitive, complex chemistry which drives the formation and alteration of UOH systems. Not only is the chemistry driven by such things as temperature, solution pH and time, the presence of multiple metal systems must also be considered. Therefore, further lab-

This journal is © The Royal Society of Chemistry 2023

oratory-based studies involving these dual-metal systems need to be carried out to better comprehend these factors.

Author contributions

Conflicts of interest

The authors are not aware of any conflict of interest.

Acknowledgements

References

1 J. Plasil, *J. Geosci.*, 2014, **59**, 99–114.

2 R. J. Baker, *Coord. Chem. Rev.*, 2014, **266–267**, 123–136.

3 S. Alyokhina, *Nucl. Eng. Technol.*, 2018, **50**, 717–723.

4 J. Janeczek and R. C. Ewing, *J. Nucl. Mater.*, 1992, **190**, 157–173.

5 J. Janeczek and R. C. Ewing, *J. Nucl. Mater.*, 1992, **190**, 128–132.

6 D. J. Wronkiewicz, J. K. Bates, S. F. Wolf and E. C. Buck, *J. Nucl. Mater.*, 1996, **238**, 78–95.

7 R. J. Finch and R. C. Ewing, *J. Nucl. Mater.*, 1992, **190**, 133–156.

8 P. C. Burns, *Structural Chemistry of Inorganic Actinide Compounds*, ed. S. V. Krivovichev, P. C. Burns and I. G. Tananaev, Elsevier, 2007, pp. 1–30.

9 P. C. Burns, R. C. Ewing and F. C. Hawthorne, *Can. Mineral.*, 1997, **35**, 1551–1570.

10 J. Plásil, *Eur. J. Mineral.*, 2018, **30**, 237–251.

11 P. C. Burns, *Can. Mineral.*, 2005, **43**, 1839–1894.

12 Y. Zhang, K. T. Lu and R. Zheng, *Dalton Trans.*, 2022, **51**, 2158–2169.

13 R. Vochten, L. Van Haverbeke and R. Sobry, *J. Mater. Chem.*, 1991, **1**, 637–642.

14 N. G. Chernorukov, O. V. Nipruk, K. A. Klinshova, O. N. Tumaeva and D. V. Sokolov, *New J. Chem.*, 2021, **45**, 9922–9922.

15 P. C. Burns and F. C. Hill, *Can. Mineral.*, 2000, **38**, 163–173.

16 R. E. Glatz, Y. Li, K.-A. Hughes, C. L. Cahill and P. C. Burns, *Can. Mineral.*, 2002, **40**, 217–224.

17 Y. Li and P. C. Burns, *Can. Mineral.*, 2000, **38**, 737–749.

18 Y. Zhang, J. Čejka, G. R. Lumpkin, T. T. Tran, I. Aharonovich, I. Karatchevtseva, J. R. Price, N. Scales and K. Lu, *New J. Chem.*, 2016, **40**, 5357–5357.

19 Y. Zhang, R. Aughterson, I. Karatchevtseva, L. Kong, T. T. Tran, J. Čejka, I. Aharonovich and G. R. Lumpkin, *New J. Chem.*, 2018, **42**, 12386–12393.

20 K.-A. Kubatko and P. C. Burns, *Inorg. Chem.*, 2006, **45**, 10277–10281.

21 Y. Li and P. C. Burns, *Can. Mineral.*, 2000, **38**, 1433–1441.

22 K. T. Lu, Y. Zhang, T. Wei, T. A. Ablott, T. H. Nguyen and R. Zheng, *New J. Chem.*, 2022, **46**, 1371–1371.

23 T. A. Ablott, K. T. Lu, R. D. Aughterson and Y. Zhang, *Dalton Trans.*, 2022, **51**, 15965–15973.

24 K. T. Lu, Y. Zhang, T. Wei, Z. Wang, D. T. Oldfield and R. Zheng, *Inorg. Chem.*, 2021, **60**, 13233–13241.

25 K. T. Lu, Y. Zhang, R. D. Aughterson and R. Zheng, *Dalton Trans.*, 2020, **49**, 15854–15863.

26 Y. Zhang, T. Wei, T. T. Tran, K. T. Lu, Z. Zhang, J. R. Price, I. Aharonovich and R. Zheng, *Inorg. Chem.*, 2020, **59**, 12166–12175.

27 C. M. Hussain and R. Keçili, *Modern Environmental Analysis Techniques for Pollutants*, ed. C. M. Hussain and R. Keçili, Elsevier, 2020, pp. 1–36.

28 A. Kubier, R. T. Wilkin and T. Pichler, *Appl. Geochem.*, 2019, **108**, 1–16.

29 R. C. Ewing, *Nat. Mater.*, 2015, **14**, 252–257.

30 M. Rivenet, N. Vigier, P. Roussel and F. Abraham, *J. Solid State Chem.*, 2009, **182**, 905–912.

31 F. Cesbron, W. L. Brown, P. Bariand and J. Geffroy, *Mineral. Mag.*, 1972, **38**, 781–789.

32 T. A. Olds, J. Plášil, A. R. Kampf, R. Škoda, P. C. Burns, J. Čejka, V. Bourgoin and J.-C. Boulliard, *Eur. J. Mineral.*, 2017, **29**, 129–141.

33 D. Aragão, J. Aishima, H. Cherukuvada, R. Clarken, M. Clift, N. P. Cowieson, D. J. Ericsson, C. L. Gee, S. Macedo, N. Mudie, S. Panjikar, J. R. Price, A. Riboldi-Tunnicliffe, R. Rostan, R. Williamson and T. T. Caradoc-Davies, *J. Synchrotron Radiat.*, 2018, **25**, 885–891.

34 W. Kabsch, *Acta Crystallogr., Sect. D: Biol. Crystallogr.*, 2010, **66**, 133–144.

35 G. M. Sheldrick, *SADABS, Empirical Absorption and Correction Software*, University of Göttingen, Göttingen, 1996.

36 G. M. Sheldrick, *Acta Crystallogr., Sect. A: Found. Adv.*, 2015, **71**, 3–8.

37 G. M. Sheldrick, *Acta Crystallogr., Sect. C: Struct. Chem.*, 2015, **71**, 3–8.

38 O. V. Dolomanov, L. J. Bourhis, R. J. Gildea, J. A. K. Howard and H. Puschmann, *J. Appl. Crystallogr.*, 2009, **42**, 339–341.

39 Y. Zhang, R. D. Aughterson, Z. Zhang, T. Wei, K. Lu, J. Čejka and I. Karatchevtseva, *Inorg. Chem.*, 2019, **58**, 10812–10821.

40 L. N. G. Chernorukov, O. V. Nipruk, K. A. Klin, G. N. Chernorukov and O. N. Tumaeva, *Radiochemistry*, 2021, **63**, 110–120.

41 N. E. Brese and M. O'Keefe, *Acta Crystallogr.*, 1991, **47**, 192–197.

42 R. M. Wood and G. J. Palenik, *Inorg. Chem.*, 1999, **38**, 1031–1034.

43 K. T. Lu, Y. Zhang, T. Wei, J. Čejka and R. Zheng, *Dalton Trans.*, 2020, **49**, 5832–5841.

44 Y. Li, C. L. Cahill and P. C. Burns, *Chem. Mater.*, 2001, **13**, 4026–4031.

45 F. C. Hill and P. C. Burns, *Can. Mineral.*, 1999, **37**, 1283–1288.

46 P. C. Burns, R. J. Finch, F. C. Hawthorne, M. L. Miller and R. C. Ewing, *J. Nucl. Mater.*, 1997, **249**, 199–206.

47 J. Plášil, R. Škoda, J. Čejka, V. Bourgoin and J.-C. Boulliard, *Eur. J. Mineral.*, 2016, **28**, 959–967.

48 P. C. Burns and R. J. Finch, *Am. Mineral.*, 1999, **84**, 1456–1460.

49 F. C. Hawthorne, R. J. Finch and R. C. Ewing, *Can. Mineral.*, 2006, **44**, 1379–1385.

50 J. L. Brugger, S. V. Krivovichev, P. Berlepsch, N. Meisser, S. Ansermet and T. Armbruster, *Am. Mineral.*, 2004, **89**, 339–347.

51 G. L. Klunder, J. W. Plaue, P. E. Spackman, P. M. Grant, R. E. Lindvall and I. D. Hutcheon, *Appl. Spectrosc.*, 2013, **67**, 1049–1056.

52 Y. Zhang, M. Bhadbhade, I. Karatchevtseva, J. R. Price, H. Liu, Z. Zhang, L. Kong, J. Čejka, K. Lu and G. R. Lumpkin, *J. Solid State Chem.*, 2015, **226**, 42–49.

53 R. L. Frost, J. Čejka, G. A. Ayoko and M. L. Weier, *Polyhedron*, 2007, **26**, 3724–3730.

54 R. L. Frost, J. Čejka and M. L. Weier, *J. Raman Spectrosc.*, 2007, **38**, 460–466.